Available online at www.sciencedirect.com
SCIENCE DIRECT®
Journal of Computational Physics 197 (2004) 624–646
JOURNAL OF COMPUTATIONAL PHYSICS
www.elsevier.com/locate/jcp

Computational modeling of ultrashort powerful laser pulses in a nonlinear crystal

Olivier Saut *

MIP, UMR 5640 (CNRS-UPS-INSA), Université Paul Sabatier, 118, route de Narbonne, 31062 Toulouse Cedex 4, France
CEA/CESTA, B.P. 2, 33114 Le Barp, France

Received 12 May 2003; received in revised form 20 May 2003; accepted 18 December 2003
Available online 22 January 2004

Abstract

This article presents a scheme for a semi-classical model of electromagnetic wave propagation in a non-centrosymmetric crystal of KDP. The model was throughfully described in [A Maxwell–Bloch model with discrete symmetries for wave propagation in nonlinear crystals: an application to KDP (submitted)]. It uses Maxwell's equations to describe the wave field and Bloch's equations for the medium at the quantum-mechanical level. We extend the Yee [Computational Electrodynamics: The Finite-difference Time-domain Method, second ed., Artech House, Boston, MA, 2000; IEEE Trans. Antennas Propag. AP-14 (1966) 302] scheme, in the undimensional case, used for isotropic media to treat the case of a KDP crystal, while ensuring an accurate scheme. Finally, several numerical simulations are performed.

1. Introduction

The development of laser able to produce ultra-short pulses requires the elaboration of new, adequate models to describe nonlinear dispersion as well as polarization effects in the wave–crystal interaction. Indeed, for powerful laser sources, classical models like systems of nonlinear Schrödinger equations [3,19] are no longer valid. For such pulses, the hypothesis of monochromatic waves is no longer relevant. This requires a time-domain description rather than a spectral one as used in classical nonlinear optics [2,3,12,17]. Besides, for some very important practical applications such as second harmonic generation in a crystal, it has become necessary to develop models to study the interplay between anisotropy and nonlinearities in a material. Several macroscopic models such as [7] describe the average response of the medium over large scales and a large assembly of atoms, and in particular over distances larger than the wavelength. At variance, microscopic models describe the response on sub-wavelength scales and account for microscopic physics in a fairly accurate way. The Bloch model is one of these microscopic models.

* Tel.: +33-561-558-583; fax: +33-561-558-385.
E-mail address: Olivier.Saut@gmm.insa-tlse.fr (O. Saut).

0021-9991/$ - see front matter
doi:10.1016/j.jcp.2003.12.016

In [4], we showed that the Bloch model could be more appropriate than classical macroscopic models when modeling wave–matter interaction in the case of ultrashort laser pulses. In [4], we have extended the Bloch model to the case of a crystal of KDP, bearing in mind that it could be extended to a large class of crystals.

In the Bloch model, the medium is described locally by a density matrix whose diagonal elements represent the population, while the off-diagonal elements represent the quantum coherences of a set of atomic states. The density matrix evolves according to both the atomic and wave-hamiltonians. While matter is treated quantum-mechanically, the wave-field is treated classically through Maxwell's equations. The model can thus be referred to as ''semi-classical'', according to the often-used terminology. The wave-hamiltonian involves the matrix of dipolar moments, which describes how matter reacts to the wave-field at the microscopic level. The model described in [4] gives us all the microscopic knowledge we need on the crystal. The next logical step is therefore to discretize this model.

The discretization of Maxwell–Bloch equations for isotropic media (e.g. gas) has already been deeply studied [5,27]. A new difficulty appears when considering anisotropic media, since some simplifications made in the isotropic case are no longer relevant. The different components of the electromagnetic field are no longer decoupled. We have to find an accurate scheme for such a material.

In physical experiments such as the study of second harmonic generation in a non-centro-symmetric crystal, the direction of propagation of the wave is not parallel to any of the optical axes of the crystal. The Maxwell equations are naturally written in a referential associated with the wave with one of its axis parallel to the direction of propagation. The dipolar moment matrix and by consequence the Bloch equations are written in a referential given by the symmetries of the crystal. That is to say, the Maxwell equations describing the evolution of the electromagnetic field and the Bloch equations describing the matter evolution are not written in the same axes. This does not ease the discretization process and we shall show how to overcome this problem.

We restrict ourselves to the case of unidimensional electromagnetic fields. The electric field $\mathbf{E}$ and the magnetic field $\mathbf{B}$ depend only on one variable in space in the direction of the incoming wave. This is a first step toward the validation of our model [4]. The bidimensional study is a work in progress [20] and will be published later.

The organization of this paper is as follows: Section 2 quickly exposes the physical context and the Maxwell–Bloch model.

In Section 3, we shall start by recalling the classical Yee scheme providing a discretization scheme for the electromagnetic field in Maxwell equations. These equations also involve the polarization, which we will then discretize. Finally, we will write a scheme for the Bloch equations describing the matter evolution. Throughout the complete discretization of the Maxwell–Bloch equations, we try to highlight the methods used to ensure a second order scheme.

In Section 4, we describe the boundary conditions we have used to perform numerical simulations.

Eventually, in Section 5, we perform several numerical experimentations to check the validity of our model.

2. Physical context

2.1. Experimental setup

In this paper, let us consider the following experimental setup. A wave-field propagates in a linear medium, before traveling through a uniaxial crystal.

The linear index of the medium is chosen to minimize the reflexion of the wave at the interfaces with the crystal.

Let us start by recalling the definition of the optical axis for a uniaxial crystal. In full generality, in any material, the coordinates of the linear polarization $\mathbf{P}^{(1)}$ are written $P_i^{(1)} = \sum_j \tilde{\boldsymbol{\varepsilon}}_{ij} E_j$, where $\tilde{\boldsymbol{\varepsilon}}$ is the two-dimensional tensor of linear susceptibility of the medium and $\mathbf{E}$ the electric field. In a uniaxial crystal, one can find a set of axes $\mathscr{R}_c = (\mathbf{u}, \mathbf{v}, \mathbf{w})$ (which we shall call the *crystalline axes*) where the linear polarization coordinates in these axes can be expressed as

$$P_i^{(1)} = \tilde{\boldsymbol{\varepsilon}}_{ii} E_i,$$

where $\tilde{\boldsymbol{\varepsilon}}_{uu} = \tilde{\boldsymbol{\varepsilon}}_{vv} \neq \tilde{\boldsymbol{\varepsilon}}_{ww}$. The direction of the vector $\mathbf{w}$ is called the *optical axis* of the crystal.

We denote by $\mathbf{z}$ (see Fig. 1) a unit vector parallel to the direction of propagation of the incoming plane wave. We consider plane waves and we shall denote by $(\mathbf{x}, \mathbf{y})$, two unit vectors spanning the plane of the wave (Fig. 1). We shall call $\mathscr{R} = (\mathbf{x}, \mathbf{y}, \mathbf{z})$ the *wave axes*. In practical experiments, the direction of propagation of the wave and the optical axis of the crystal are not parallel. For instance, the phase matching condition for harmonic generation can be satisfied by rotating the crystal. Once rotated, the crystal is cut to ensure a normal incidence of the wave as shown in Fig. 1.

2.2. Maxwell equations

The incoming plane wave is represented by the pair $(\mathbf{E}, \mathbf{B})$, where $\mathbf{E}$ is the electric field and $\mathbf{B}$ the magnetic induction. The fields $\mathbf{E}$ and $\mathbf{B}$ obey the Maxwell equations:

$$\begin{aligned} &\partial_t \mathbf{B} = -\mathrm{rot}\ \mathbf{E}, \\ &\partial_t \mathbf{E} = \frac{1}{\mu_0} \boldsymbol{\varepsilon}^{-1} \mathrm{rot}\ \mathbf{B} - \boldsymbol{\varepsilon}^{-1} \partial_t \mathbf{P}, \\ &\mathrm{div}\ \mathbf{B} = 0, \\ &\mathrm{div}\ \mathbf{D} = 0, \end{aligned} \tag{2.1}$$

where $\boldsymbol{\varepsilon}$ is the static linear tensor of the medium in which the wave travels. We recall that $\mathbf{D} = \boldsymbol{\varepsilon}\mathbf{E} + \mathbf{P}$. The tensor $\boldsymbol{\varepsilon}$ is diagonal in the crystalline axes $\mathscr{R}_c$, but for instance in the wave axes $\mathscr{R}$ it may have far more non-vanishing coefficients.

The interaction with the crystal is modeled by the polarization $\mathbf{P}$, which is obtained through the Bloch equation (2.5).

The waves propagate along the direction z (see Fig. 1) and we shall make the assumption that the fields $\mathbf{E}$ and $\mathbf{B}$ depend only on the z variable in space. Then, the previous system (2.1) can be simplified as

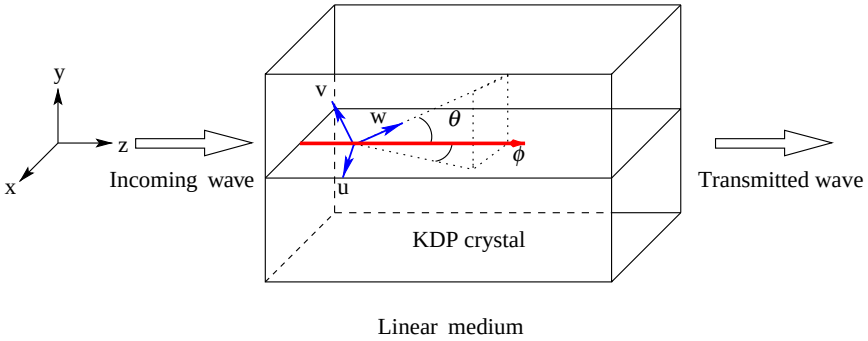

Fig. 1. Geometry of the experiment.

$$
\begin{aligned}
&\partial_t B_x = \partial_z E_y,\\
&\partial_t B_y = -\partial_z E_x,\\
&\partial_t E_x = \frac{1}{\mu_0}\left[-\left(\boldsymbol{\varepsilon}^{-1}\right)_{xx}\partial_z B_y + \left(\boldsymbol{\varepsilon}^{-1}\right)_{xy}\partial_z B_x\right] - \left(\boldsymbol{\varepsilon}^{-1}\right)_{xx}\partial_t P_x - \left(\boldsymbol{\varepsilon}^{-1}\right)_{xy}\partial_t P_y - \left(\boldsymbol{\varepsilon}^{-1}\right)_{xz}\partial_t P_z,\\
&\partial_t E_y = \frac{1}{\mu_0}\left[\left(\boldsymbol{\varepsilon}^{-1}\right)_{yy}\partial_z B_x - \left(\boldsymbol{\varepsilon}^{-1}\right)_{yx}\partial_z B_y\right] - \left(\boldsymbol{\varepsilon}^{-1}\right)_{yx}\partial_t P_x - \left(\boldsymbol{\varepsilon}^{-1}\right)_{yy}\partial_t P_y - \left(\boldsymbol{\varepsilon}^{-1}\right)_{yz}\partial_t P_z,\\
&\partial_z B_z = 0,\\
&\partial_z D_z = 0.
\end{aligned}
$$

Remark 1. According to the Maxwell equations, the third component B_z of the magnetic field has to verify $\partial_z B_z = \partial_t B_z = 0$. Thus we do not need to compute this coordinate of the magnetic field. The Ampère equations on E_z does not yield anything more on E_z than the equation $\partial_z D_z = 0$.

2.3. Bloch equations

We use a quantum model to represent the crystal. A quantum system is represented by a wave-function ψ (see [21] for instance). The evolution of ψ is driven by the Schrödinger equation:

$$\mathrm{i}\hbar\partial_t\psi = \mathscr{H}\psi,$$

where the Hamiltonian $\mathscr{H}$ is classically decomposed in $\mathscr{H} = H_0 + V$, H_0 being the free Hamiltonian and V the potential resulting from the action of the electromagnetic field.

Let us first introduce some notations. We make the assumption that the free Hamiltonian H_0 has N distinct eigenvalues: $\mathscr{E}_1 = \hbar\omega_1, \ldots, \mathscr{E}_N = \hbar\omega_N$. For convenience, we write $\omega_{nm} = \omega_n - \omega_m$.

We shall denote by d_n the multiplicity of the eigenvalue $\mathscr{E}_n$. For each level n, we choose a basis of eigenstates $(\psi_{(n,1)}, \ldots, \psi_{(n,d_n)})$. For each pair of eigenstates $(\psi_{(l,r)}, \psi_{(m,s)})$, we can compute

$$\boldsymbol{\mu}_{(l,r)(m,s)} \equiv \langle \psi_{(l,r)}, \mathbf{r}\psi_{(m,s)}\rangle, \tag{2.2}$$

where $\langle , \rangle$ is the canonical inner product and $\mathbf{r}$ is the position operator. The matrix $\boldsymbol{\mu}$ is called the *dipolar matrix*. It is a square matrix of dimension $\sum_n d_n$ whose coefficients are vectors in $\mathbb{C}^3$. It shall be noted that the dipolar matrix depends on the chosen referential for the position operator $\mathbf{r}$. In [4], we have computed the dipolar matrix for the KDP in the crystalline axes $\mathscr{R}_c$. Indeed in the crystalline axes, the symmetries of the crystal translate into vanishing coefficients of the dipolar matrix $\boldsymbol{\mu}$.

In the dipolar approximation, V is given by

$$V = -\boldsymbol{\mu}\cdot\mathbf{E}. \tag{2.3}$$

Let us now introduce a statistical description of the system since a large number of atoms interact with the wave. We introduce the density matrix ρ described in [21] for instance. Let us recall that the diagonal elements of the density matrix represent the population levels of the corresponding eigenspace of the free Hamiltonian, while the off-diagonal terms represent the coherences between these levels.

It is straightforward (e.g. see [8]) to show that the density matrix ρ obeys the Bloch equations:

$$\partial_t\rho_{jk} = -\mathrm{i}(\omega_j - \omega_k)\rho_{jk} - \frac{\mathrm{i}}{\hbar}[V,\rho]_{jk} = -\mathrm{i}\omega_{jk}\rho_{jk} + \frac{\mathrm{i}}{\hbar}[\boldsymbol{\mu}\cdot\mathbf{E},\rho]_{jk} \tag{2.4}$$

for all $1 \leqslant j,k \leqslant N$, where we recall $[A,B] = AB - BA$.

Remark 2. Eq. (2.5) does not include phenomenological relaxation terms to render spontaneous emission of light, vibrations in crystal lattices. This would not add any complexity to the derivation of the scheme (see in [6] several methods for including these phenomena in the Bloch equations). Besides, in the time-scale we are considering, the relaxation effects would have been negligible.

To simplify the equations, we introduce the operator Rn defined by $\mathrm{Rn}(\rho)_{jk} = -\mathrm{i}\omega_{jk}\rho_{jk}$. The two sets of Eqs. (2.1) and (2.5) are related by the polarization $\mathbf{P}$ which is given by

$$\mathbf{P} = \mathscr{N}\,\mathrm{tr}\,(\boldsymbol{\mu}\rho), \tag{2.5}$$

where $\mathscr{N}$ is the density of molecules per unit volume.

Hence Eqs. (2.1), (2.4) and (2.5) form a closed system.

2.4. Equations rotation

The two systems (2.1) and (2.5) are written in two different sets of axes. Indeed, the Maxwell equations are naturally expressed in a referential ($\mathscr{R}$) associated with the direction of propagation of the wave. The Bloch equations are written in the referential ($\mathscr{R}_c$) chosen for the dipolar moment matrix $\boldsymbol{\mu}$. Furthermore, the tensor $\boldsymbol{\varepsilon}$ involved in the Maxwell equations is diagonal in $\mathscr{R}_c$.

We could have kept both equations in their respective axes but then, we would have had to rotate the electric field $\mathbf{E}$ and the polarization $\mathbf{P}$ for each time-step before solving the Bloch (2.5) or Maxwell (2.1) equations.

We could also have written both equations in the crystalline axes $\mathscr{R}_c$. Since the tensor $\boldsymbol{\varepsilon}$ (or its inverse) is diagonal in $\mathscr{R}_c$, there would have been only be one coordinate of the polarization involved in each of the Ampère equations. Yet the space-derivatives of the electromagnetic field would have become far more complex to express.

That is why we have eventually chosen to write the Bloch equation (2.5) in the wave axes $\mathscr{R}$. The main drawback of this approach is that the tensor $\boldsymbol{\varepsilon}$ involved in Maxwell equations (2.1) is not necessarily diagonal. We will see how to reduce the number of its non-vanishing terms.

The dipolar matrix $\boldsymbol{\mu}$ depends on the chosen axes. In Eq. (2.5) the space variable acts as a parameter and only the time-derivatives of the density matrix ρ appear in (2.5). Hence to write Eq. (2.5) in the correct referential, we only need to rotate the dipolar matrix $\boldsymbol{\mu}$ given by Eq. (2.2). That is we just have to rotate the position operator. Let R be a rotation. The dipolar matrix in the referential $R(\mathscr{R}_c)$ is the matrix $\tilde{\boldsymbol{\mu}} = (R^{-1}\mu_{ij})_{ij}$. To write the Bloch equations in $R(\mathscr{R}_c)$, we take $\tilde{\boldsymbol{\mu}}$ as the dipolar matrix.

Now we show how to choose the two vectors $(\mathbf{x}, \mathbf{y})$ spanning the plane wave, to maximize the number of vanishing coefficients of the tensor $\boldsymbol{\varepsilon}$ and its inverse.

Let us first define θ as the angle between the extraordinary axis $\mathbf{w}$ of the crystal and the direction of propagation $\mathbf{z}$ of the wave. We denote by $\mathbf{z}^*$, the projection of $\mathbf{z}$ on the plane $\langle \mathbf{u}, \mathbf{v} \rangle$. We can then define the angle ϕ between $\mathbf{u}$ and $\mathbf{z}^*$.

We define the following vectors by their coordinates on $\mathscr{R}_c$

$$\mathbf{x} = \begin{pmatrix} \cos\theta\cos\phi \\ \cos\theta\sin\phi \\ -\sin\theta \end{pmatrix},$$

$$\mathbf{y} = \begin{pmatrix} -\sin\phi \\ \cos\phi \\ 0 \end{pmatrix}.$$

The two vectors $(\mathbf{x}, \mathbf{y})$ span the wave plane.

Now we give the form of the tensor $\boldsymbol{\varepsilon}$ in the referential $\mathscr{R} = (\mathbf{x}, \mathbf{y}, \mathbf{z})$. In $\mathscr{R}_c$ its expression is

$$\boldsymbol{\varepsilon} = \begin{pmatrix} \varepsilon_\perp & 0 & 0 \\ 0 & \varepsilon_\perp & 0 \\ 0 & 0 & \varepsilon_\parallel \end{pmatrix},$$

where $\varepsilon_\perp$ and $\varepsilon_\parallel$ are two real numbers.

Given the rotation matrix from $\mathscr{R}_c$ to $\mathscr{R}$, we can write its expression in the wave axes $\mathscr{R}$:

$$\boldsymbol{\varepsilon} = \begin{pmatrix} \varepsilon_\perp \cos^2\theta + \varepsilon_\parallel \sin^2\theta & 0 & \cos\theta \sin\theta(\varepsilon_\perp - \varepsilon_\parallel) \\ 0 & \varepsilon_\perp & 0 \\ \cos\theta \sin\theta(\varepsilon_\perp - \varepsilon_\parallel) & 0 & \varepsilon_\perp \sin^2\theta + \varepsilon_\parallel \cos^2\theta \end{pmatrix},$$

its inverse is given by

$$\boldsymbol{\eta} \equiv \boldsymbol{\varepsilon}^{-1} = \begin{pmatrix} \frac{\varepsilon_\perp \sin^2\theta + \varepsilon_\parallel \cos^2\theta}{\varepsilon_\perp \varepsilon_\parallel} & 0 & -\frac{\cos\theta \sin\theta(\varepsilon_\perp - \varepsilon_\parallel)}{\varepsilon_\perp \varepsilon_\parallel} \\ 0 & \frac{1}{\varepsilon_\perp} & 0 \\ -\frac{\cos\theta \sin\theta(\varepsilon_\perp - \varepsilon_\parallel)}{\varepsilon_\perp \varepsilon_\parallel} & 0 & \frac{\varepsilon_\perp \cos^2\theta + \varepsilon_\parallel \sin^2\theta}{\varepsilon_\perp \varepsilon_\parallel} \end{pmatrix}.$$

By carefully choosing the axes, we were able to cancel four terms of the static tensor $\boldsymbol{\varepsilon}$.

2.5. Summary of the equations to be solved

From the equation $\operatorname{div} \mathbf{D} = 0$, we get $\partial_z D_z = 0$. Thus the third component of the vector $\mathbf{D}$ does not depend on the space variable z. We take $D_z(z = 0) = 0$, then $D_z = 0\,\forall z$. Using the expression of $\mathbf{D}$, we get an expression of E_z,

$$E_z = \frac{-P_z - \varepsilon_{zx} E_x - \varepsilon_{zy} E_y}{\varepsilon_{zz}},$$

since $\mathbf{D} = \boldsymbol{\varepsilon}\mathbf{E} + \mathbf{P}$. The magnetic field satisfies $\partial_z B_z = 0$, we choose to set $B_z(z = 0) = 0$, so $B_z = 0$, $\forall z$.

As we have shown, by choosing an adequate expression of the rotation, we can cancel some terms of the tensor $\boldsymbol{\varepsilon}$. Then, the system can be simplified a little more.

The equations describing the evolution of the first two coordinates of the electric field $\mathbf{E}$ become

$$\begin{aligned} \partial_t E_x &= -\frac{\eta_{xx}}{\mu_0} \partial_z B_y - \eta_{xx} \partial_t P_x - \eta_{xz} \partial_t P_z, \\ \partial_t E_y &= \frac{\eta_{yy}}{\mu_0} \partial_z B_x - \eta_{yy} \partial_t P_y. \end{aligned} \tag{2.6}$$

The third component of the electric field $\mathbf{E}$ is given by

$$E_z = \frac{-P_z - \varepsilon_{zx} E_x}{\varepsilon_{zz}}. \tag{2.7}$$

In Eqs. (2.6) and (2.7), the polarization term is obtained from the Bloch equation (2.5)

$$\partial_t \rho_{jk} = -\mathrm{i}\omega_{jk} \rho_{jk} + \frac{\mathrm{i}}{\hbar} [\boldsymbol{\mu} \cdot \mathbf{E}, \rho]_{jk}, \quad 1 \leqslant j, k \leqslant N,$$

by $\mathbf{P} = \mathscr{N} \operatorname{tr}(\boldsymbol{\mu}\rho)$.

The magnetic field **B** evolves with the equations

$$\begin{aligned} \partial_t B_x &= \partial_z E_y, \\ \partial_t B_y &= -\partial_z E_x. \end{aligned} \tag{2.8}$$

We do not need to compute the last coordinate of the magnetic field since $B_z = 0$.

3. Discretization

In the previous section, we wrote the system of equations that we now intend to solve numerically. Before proceeding with numerical experimentations, we need a scheme for discretizing these equations. We also wish to keep a second order scheme. Let us start with a classical part: the Yee scheme [23,25]. In order to ensure a second order scheme, we should however proceed carefully when coupling the Maxwell (2.1) and Bloch (2.5) equations, as can be seen in the final part of this section.

3.1. A scheme for the Maxwell equations

We need a scheme for the Maxwell equations (2.1). As stated before, our scheme is based on the classical Yee scheme [25] but needs to be adapted to include the polarization **P** and the density matrix ρ.

Classically, we discretize the electric field **E** and the magnetic field **B** shifted by half a step in time as in Fig. 2.

The polarization **P** is estimated on the same points as the electric field **E** and ρ on the same points as the magnetic field **B** (see Fig. 2).

For a function u defined on the grid, we write $u^{n,m}$ for the value of u at the grid point (z^m, t^n) where $t^n = n\delta t$, $z^m = m\delta z$. We also use the notation $v^{n,m}$ for $v(z^m, t^n)$ when v is defined for continuously varying (z, t).

The Faraday equations (2.8) do not depend on ρ, they are easily discretized

$$\begin{aligned} \frac{B_x^{n+\frac{1}{2}} - B_x^{n-\frac{1}{2}}}{\delta t} &= \partial_z E_y^n, \\ \frac{B_y^{n+\frac{1}{2}} - B_y^{n-\frac{1}{2}}}{\delta t} &= -\partial_z E_x^n, \end{aligned} \tag{3.1}$$

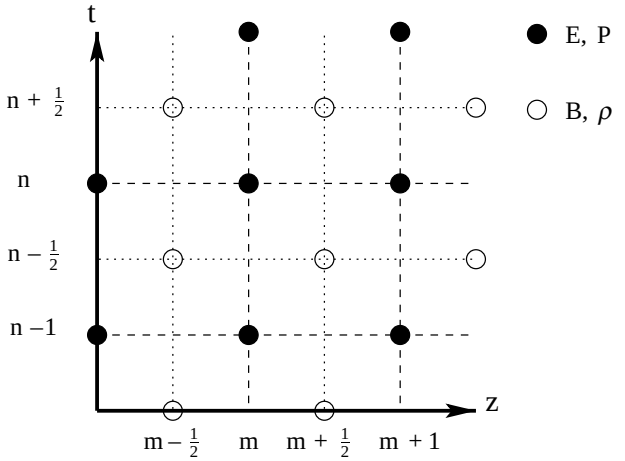

Fig. 2. Yee's scheme.

which gives us a scheme of order 2. Hence, given the electric field $\mathbf{E}^n$ at time t^n, we can compute the magnetic field $\mathbf{B}^{n+\frac{1}{2}}$ at time $t^{n+\frac{1}{2}}$.

We then write the Ampère equations (2.6) for time $t^{n+\frac{1}{2}}$:

$$\begin{aligned}\frac{E_x^{n+1}-E_x^n}{\delta t} &= \frac{1}{\mu_0}\left(-\eta_{xx}\partial_z B_y^{n+\frac{1}{2}}\right) - \eta_{xx}(\partial_t P_x)^{n+\frac{1}{2}} - \eta_{xz}(\partial_t P_z)^{n+\frac{1}{2}},\\ \frac{E_y^{n+1}-E_y^n}{\delta t} &= \frac{1}{\mu_0}\left(\eta_{yy}\partial_z B_x^{n+\frac{1}{2}}\right) - \eta_{yy}(\partial_t P_y)^{n+\frac{1}{2}}.\end{aligned} \tag{3.2}$$

The terms corresponding to the polarization are still to be determined. They relate the wave with the crystal and, through the Bloch equations, involve the electric field $\mathbf{E}$. The time derivation of the polarization $\mathbf{P}$ is not discretized. We will compute the explicit derivative before taking its value. The various methods used to discretize the polarization term obtained through the Bloch equations were described in [5].

The space discretization is straightforward, as we describe later on.

3.2. The discretization of the polarization field

Up to now, we have used the classical scheme of Yee. In this section, we will show how to discretize the polarization $\mathbf{P}$ and the density matrix ρ to obtain a scheme of order 2 for the Maxwell–Bloch system. This is far more complex to achieve than in the isotropic case (as already described in [5]).

In our case, the polarization is not necessarily parallel to the electric field and its time-derivatives appearing in (2.6) depend on the electric field. Furthermore, the two directions x and y are no longer independent.

Let us begin with the Ampère equations (2.6), which involve the polarization. We first compute the expression of time-derivative of the polarization $\partial_t\mathbf{P}$ as a function of the electric field $\mathbf{E}$ and the density matrix ρ.

Let us recall that the polarization $\mathbf{P} = (P_x, P_y, P_z)$ is given by

$$\begin{aligned}P_x &= \mathcal{N}\,\mathrm{tr}\,(\mu_x\rho),\\ P_y &= \mathcal{N}\,\mathrm{tr}\,(\mu_y\rho),\\ P_z &= \mathcal{N}\,\mathrm{tr}\,(\mu_z\rho).\end{aligned}$$

We are interested in the time-derivatives of the polarization. To express the polarization $\mathbf{P}$, we use the Bloch equation (2.5). We have

$$\partial_t P_d = \mathcal{N}\,\mathrm{tr}\,(\mu_d\partial_t\rho), \quad d \in \{x,y,z\},$$

then the Bloch equations give us

$$\partial_t P_d = \mathcal{N}\,\mathrm{tr}\,(\mu_d \mathrm{Rn}(\rho)) - \frac{\mathrm{i}\mathcal{N}}{\hbar}\,\mathrm{tr}\,(\mu_d[V,\rho]), \quad d \in \{x,y,z\}.$$

We write the previous equation at $t^{n+\frac{1}{2}}$,

$$(\partial_t P_d)^{n+\frac{1}{2}} = \mathcal{N}\,\mathrm{tr}\,(\mu_d \mathrm{Rn}(\rho^{n+\frac{1}{2}})) - \frac{\mathrm{i}\mathcal{N}}{\hbar}\,\mathrm{tr}\,(\mu_d[V^{n+\frac{1}{2}},\rho^{n+\frac{1}{2}}]). \tag{3.3}$$

We have to compute the value of the potential $\mathbf{V}$, which involves the electric field and the dipolar moment matrix, at time $t^{n+\frac{1}{2}}$. The potential $V^{n+\frac{1}{2}}$ is given by

$$\mathbf{V}^{n+\frac{1}{2}} = \frac{\mathbf{V}^{n+1}+\mathbf{V}^n}{2},$$

hence it is obtained from $\mathbf{E}^n$ and $\mathbf{E}^{n+1}$, the approximation of the electric field $\mathbf{E}^{n+\frac{1}{2}}$ at time $t^{n+\frac{1}{2}}$ being $\frac{1}{2}(\mathbf{E}^n + \mathbf{E}^{n+1})$.

Replacing the potential $\mathbf{V}$ by its expression, we can develop Eq. (3.3)

$$(\partial_t P_d)^{n+\frac{1}{2}} = \mathcal{N}\,\mathrm{tr}\,(\mu_d \mathrm{Rn}(\rho^{n+\frac{1}{2}})) + \frac{\mathrm{i}\mathcal{N}}{\hbar}\frac{E_x^n + E_x^{n+1}}{2}\,\mathrm{tr}\,(\mu_d[\mu_x, \rho^{n+\frac{1}{2}}]) + \frac{\mathrm{i}\mathcal{N}}{\hbar}\frac{E_y^n + E_y^{n+1}}{2}\,\mathrm{tr}\,(\mu_d[\mu_y, \rho^{n+\frac{1}{2}}]) + \frac{\mathrm{i}\mathcal{N}}{\hbar}\frac{E_z^n + E_z^{n+1}}{2}\,\mathrm{tr}\,(\mu_d[\mu_z, \rho^{n+\frac{1}{2}}]).$$

At this stage, we need to compute the value $\rho^{n+\frac{1}{2}}$ of the density matrix at time $t^{n+\frac{1}{2}}$. This implies solving the Bloch equations, as will be shown this in the next section. For the time being, we shall make the assumption that $\rho^{n+\frac{1}{2}}$ is known.

Yet, the third component of the electric field $\mathbf{E}$ is not given by the Ampère equations. We need another equation to compute E_z^{n+1}. We then use Eq. (2.7):

$$E_z^{n+1} = \frac{-P_z^{n+1} - \varepsilon_{zx}E_x^{n+1}}{\varepsilon_{zz}}.$$

Moreover the polarization P_z is given by

$$P_z^{n+1} = P_z^n + \delta t(\partial_t P_z)^{n+\frac{1}{2}},$$

which is a second order approximation.

As before, we take(3.3):

$$(\partial_t P_z)^{n+\frac{1}{2}} = \mathcal{N}\,\mathrm{tr}\,(\mu_z \mathrm{Rn}(\rho^{n+\frac{1}{2}})) - \frac{\mathrm{i}\mathcal{N}}{\hbar}\,\mathrm{tr}\,(\mu_z[V^{n+\frac{1}{2}}, \rho^{n+\frac{1}{2}}]).$$

Remark 3. The term $(\partial_t P_z)^{n+\frac{1}{2}}$ does not depend on E_z since we have:

$$\mathrm{tr}(\mu_z[E_z\mu_z, \rho]) = E_z\,\mathrm{tr}\,(\mu_z[\mu_z, \rho]) = E_z\,\mathrm{tr}\,(\mu_z^2\rho - \mu_z\rho\mu_z) = 0.$$

Hence, to express E_z, we get

$$E_z^{n+1} = \frac{-P_z^n - \delta t\mathcal{N}\,\mathrm{tr}\,(\mu_z \mathrm{Rn}(\rho^{n+\frac{1}{2}})) + \frac{\mathrm{i}\delta t\mathcal{N}}{\hbar}\,\mathrm{tr}\,(\mu_z[V^{n+\frac{1}{2}}, \rho^{n+\frac{1}{2}}]) - \varepsilon_{zx}E_x^{n+1}}{\varepsilon_{zz}}.$$

Once again, we need to replace the potential $\mathbf{V}^{n+\frac{1}{2}}$ by its expression as a function of the dipolar moment matrix $\boldsymbol{\mu}$ and the electric field $\mathbf{E}^{n+\frac{1}{2}}$ at time $t^{n+\frac{1}{2}}$. The term $\mathrm{tr}\,(\mu_z[V^{n+\frac{1}{2}}, \rho^{n+\frac{1}{2}}])$ gives

$$\mathrm{tr}\,(\mu_z[V^{n+\frac{1}{2}}, \rho^{n+\frac{1}{2}}]) = -\frac{E_x^n + E_x^{n+1}}{2}\,\mathrm{tr}\,(\mu_z[\mu_x, \rho^{n+\frac{1}{2}}]) - \frac{E_y^n + E_y^{n+1}}{2}\,\mathrm{tr}\,(\mu_z[\mu_y, \rho^{n+\frac{1}{2}}]).$$

To simplify the expressions, let us introduce the following notation:

$$T_{d,d'}^{n+\frac{1}{2}} \equiv \frac{\mathrm{i}\mathcal{N}}{2\hbar}\,\mathrm{tr}\,(\mu_d[\mu_{d'}, \rho^{n+\frac{1}{2}}]),$$

$$T_d^{n+\frac{1}{2}} \equiv \mathcal{N}\,\mathrm{tr}\,(\mu_d \mathrm{Rn}(\rho^{n+\frac{1}{2}})),$$

where $d, d' \in \{x, y, z\}$.

It thus becomes easier to read the expression of E_z^{n+1}:

$$E_z^{n+1} = \frac{-\delta t\, T_{z,x}^{n+\frac{1}{2}} - \varepsilon_{zx}}{\varepsilon_{zz}} E_x^{n+1} - \frac{\delta t\, T_{z,y}^{n+\frac{1}{2}}}{\varepsilon_{zz}} E_y^{n+1} - \frac{P_z^n}{\varepsilon_{zz}} - \frac{\delta t\, T_z^{n+\frac{1}{2}}}{\varepsilon_{zz}} - \frac{\delta t\, T_{z,x}^{n+\frac{1}{2}}}{\varepsilon_{zz}} E_x^n - \frac{\delta t\, T_{z,y}^{n+\frac{1}{2}}}{\varepsilon_{zz}} E_y^n.$$

We can then write the time derivatives of the polarization as functions of the electric field:

$$\begin{aligned}(\partial_t P_x)^{n+\frac{1}{2}} = & -T_{x,z}^{n+\frac{1}{2}} \frac{\delta t\, T_{z,x}^{n+\frac{1}{2}} + \varepsilon_{zx}}{\varepsilon_{zz}} E_x^{n+1} + \left(T_{x,y}^{n+\frac{1}{2}} - T_{x,z}^{n+\frac{1}{2}} \frac{\delta t\, T_{z,y}^{n+\frac{1}{2}}}{\varepsilon_{zz}} \right) E_y^{n+1} - \frac{T_{x,z}^{n+\frac{1}{2}}}{\varepsilon_{zz}} P_z^n + T_{x,z}^{n+\frac{1}{2}} E_z^n \\ & + T_x^{n+\frac{1}{2}} - T_{x,z}^{n+\frac{1}{2}} \frac{\delta t}{\varepsilon_{zz}} T_z^{n+\frac{1}{2}} - T_{x,z}^{n+\frac{1}{2}} \frac{\delta t\, T_{z,x}^{n+\frac{1}{2}}}{\varepsilon_{zz}} E_x^n + \left(T_{x,y}^{n+\frac{1}{2}} - T_{x,z}^{n+\frac{1}{2}} \frac{\delta t\, T_{z,y}^{n+\frac{1}{2}}}{\varepsilon_{zz}} \right) E_y^n,\end{aligned}$$

$$\begin{aligned}(\partial_t P_y)^{n+\frac{1}{2}} = & \left(T_{y,x}^{n+\frac{1}{2}} - T_{y,z}^{n+\frac{1}{2}} \frac{\delta t\, T_{z,x}^{n+\frac{1}{2}} + \varepsilon_{zx}}{\varepsilon_{zz}} \right) E_x^{n+1} - T_{y,z}^{n+\frac{1}{2}} \frac{\delta t\, T_{z,y}^{n+\frac{1}{2}}}{\varepsilon_{zz}} E_y^{n+1} - \frac{T_{y,z}^{n+\frac{1}{2}}}{\varepsilon_{zz}} P_z^n + T_{y,z}^{n+\frac{1}{2}} E_z^n \\ & + T_y^{n+\frac{1}{2}} - T_{y,z}^{n+\frac{1}{2}} \frac{\delta t}{\varepsilon_{zz}} T_z^{n+\frac{1}{2}} + \left(T_{y,x}^{n+\frac{1}{2}} - T_{y,z}^{n+\frac{1}{2}} \frac{\delta t\, T_{z,x}^{n+\frac{1}{2}}}{\varepsilon_{zz}} \right) E_x^n - T_{y,z}^{n+\frac{1}{2}} \frac{\delta t\, T_{z,y}^{n+\frac{1}{2}}}{\varepsilon_{zz}} E_y^n,\end{aligned}$$

$$(\partial_t P_z)^{n+\frac{1}{2}} = T_{z,x}^{n+\frac{1}{2}} E_x^{n+1} + T_{z,y}^{n+\frac{1}{2}} E_y^{n+1} + T_z^{n+\frac{1}{2}} + T_{z,x}^{n+\frac{1}{2}} E_x^n + T_{z,y}^{n+\frac{1}{2}} E_y^n.$$

3.3. The Bloch equations

We now use a modified version of the method described in [5] to keep a second-order scheme. We solve the Bloch equations with a splitting scheme.

Let us recall that the density matrix ρ is driven by Eq. (2.5)

$$\partial_t \rho_{jk} = -\mathrm{i}\omega_{jk}\rho_{jk} - \frac{\mathrm{i}}{\hbar}[\mathbf{V}, \rho]_{jk}$$

for all $1 \leqslant j, k \leqslant N$.

We solve separately each of its components. We start with the operator corresponding to the interaction of the electric field $\mathbf{E}$ on the medium, and thus we consider the equation

$$\partial_t \rho = -\frac{\mathrm{i}}{\hbar}[\mathbf{V}, \rho]. \tag{3.4}$$

Eq. (3.4) is solved exactly by

$$\rho(t) = \mathrm{e}^{-\frac{\mathrm{i}}{\hbar}\int_0^t \mathbf{V}(s)\,\mathrm{d}s} \rho(0) \mathrm{e}^{\frac{\mathrm{i}}{\hbar}\int_0^t \mathbf{V}(s)\,\mathrm{d}s}.$$

Numerically, we have to approximate the integral and the exponential terms. The integral is approached by the centered rectangles method which is of order 2

$$\int_{(n-\frac{1}{2})\delta t}^{(n+\frac{1}{2})\delta t} V(s)\,\mathrm{d}s \sim \delta t V^n.$$

Given a matrix M, we approach its exponential by

$$\exp M \sim \left(I - \frac{1}{2}M\right)^{-1}(I + \frac{1}{2}M),$$

which is also a second order approximation of the exponential.

We shall call $S_{\mathscr{H}}$, the solving operator of this part of the splitting.

We now solve the part of Eq. (2.5) involving the free hamiltonian. We have to solve

$$\partial_t \rho_{jk} = -\mathrm{i}\omega_{jk}\rho_{jk}$$

for all $1 \leqslant j, k \leqslant N$. The explicit solution is clearly

$$\rho_{jk}(t) = \exp(-\mathrm{i}\omega_{jk}t)\rho_{jk}(0).$$

Remark 4. Since there is no relaxation terms in the equations, the atomic populations (diagonal terms of the density matrix ρ) only evolve through the action of the electric field **E**.

We shall call $S_{\mathscr{H}_0}$, the solving operator of this part of the splitting.

As we wish to obtain an accurate overall scheme, we use a Strang method, which is of order 2

$$\rho^{n+\frac{1}{2}} = S^{\frac{1}{2}}_{\mathscr{H}_0} S_{\mathscr{H}} S^{\frac{1}{2}}_{\mathscr{H}_0} \rho^{n-\frac{1}{2}}. \tag{3.5}$$

3.4. Final scheme

Collecting the above equations, Eq. (2.8) becomes

$$\frac{B_x^{n+\frac{1}{2},m+\frac{1}{2}} - B_x^{n-\frac{1}{2},m+\frac{1}{2}}}{\delta t} = \frac{E_y^{n,m+1} - E_y^{n,m}}{\delta z},$$
$$\frac{B_y^{n+\frac{1}{2},m+\frac{1}{2}} - B_y^{n-\frac{1}{2},m+\frac{1}{2}}}{\delta t} = -\frac{E_x^{n,m+1} - E_x^{n,m}}{\delta z}.$$

For the Bloch equation (2.5), the space variable z acts as a parameter, as we discretized ρ on the same points as **E**.

The system (3.2) then becomes

$$\frac{E_x^{n+1,m} - E_x^{n-1,m}}{\delta t} = \frac{1}{\mu_0}\left(-\eta_{xx}\frac{B_y^{n+\frac{1}{2},m+\frac{1}{2}} - B_y^{n+\frac{1}{2},m-\frac{1}{2}}}{\delta z}\right) - \eta_{xx}(\partial_t P_x)^{n+\frac{1}{2},m} - \eta_{xz}(\partial_t P_z)^{n+\frac{1}{2},m},$$

$$\frac{E_y^{n+1,m} - E_y^{n-1,m}}{\delta t} = \frac{1}{\mu_0}\left(\eta_{yy}\frac{B_x^{n+\frac{1}{2},m+\frac{1}{2}} - B_x^{n+\frac{1}{2},m-\frac{1}{2}}}{\delta z}\right) - \eta_{yy}(\partial_t P_y)^{n+\frac{1}{2},m},$$

the polarization terms do not involve space derivatives, and we replace the space-derivatives of the magnetic field by their discretized expression in system (3.6).

Then, we replace the time-derivatives of the polarization **P** by their expressions in the Ampère equations (3.2):

$$E_x^{n+1,m} = \delta t\left(\eta_{xx}\frac{\delta t\, T_{z,x}^{n+\frac{1}{2},m}+\varepsilon_{zx}}{\varepsilon_{zz}}T_{x,z}^{n+\frac{1}{2},m}-\eta_{xz}T_{z,x}^{n+\frac{1}{2},m}\right)E_x^{n+1,m}$$
$$-\delta t\left(\eta_{xx}\left[T_{x,y}^{n+\frac{1}{2},m}-T_{x,z}^{n+\frac{1}{2},m}\frac{\delta t\, T_{z,y}^{n+\frac{1}{2},m}}{\varepsilon_{zz}}\right]+\eta_{xz}T_{z,y}^{n+\frac{1}{2},m}\right)E_y^{n+1,m}+\gamma_x^{n+\frac{1}{2},m},$$

$$E_y^{n+1,m} = -\delta t\left(\eta_{yy}\left[T_{y,x}^{n+\frac{1}{2},m}-T_{y,z}^{n+\frac{1}{2},m}\frac{\delta t\, T_{z,x}^{n+\frac{1}{2},m}+\varepsilon_{zx}}{\varepsilon_{zz}}\right]\right)E_x^{n+1,m}+\delta t\left(\eta_{yy}T_{y,z}^{n+\frac{1}{2},m}\frac{\delta t\, T_{z,y}^{n+\frac{1}{2},m}}{\varepsilon_{zz}}\right)E_y^{n+1,m}+\gamma_y^{n+\frac{1}{2},m},$$

where $\gamma_x^{n+\frac{1}{2},m}$ and $\gamma_y^{n+\frac{1}{2},m}$ are terms depending only on variables computed before time $t^{n+\frac{1}{2}}$. They are given by:

$$\gamma_x^{n+\frac{1}{2},m} = E_x^{n,m}+\frac{\delta t}{\mu_0}\left(-\eta_{xx}\frac{B_y^{n+\frac{1}{2},m+\frac{1}{2}}-B_y^{n+\frac{1}{2},m-\frac{1}{2}}}{\delta z}\right)-\eta_{xx}\delta t\, T_x^{n+\frac{1}{2},m}-\eta_{xz}\delta t\, T_z^{n+\frac{1}{2},m}$$
$$+\delta t\left[\eta_{xx}\left(\frac{P_z^{n,m}}{\varepsilon_{zz}}-E_z^{n,m}\right)T_{x,z}^{n+\frac{1}{2},m}\right]+\delta t\left(\eta_{xx}\frac{\delta t\, T_{z,x}^{n+\frac{1}{2},m}}{\varepsilon_{zz}}T_{x,z}^{n+\frac{1}{2},m}-\eta_{xz}T_{z,x}^{n+\frac{1}{2},m}\right)E_x^{n,m}$$
$$+(\delta t)^2\frac{\eta_{xx}}{\varepsilon_{zz}}T_{x,z}^{n+\frac{1}{2},m}T_z^{n+\frac{1}{2},m}-\delta t\left(\eta_{xx}\left[T_{x,y}^{n+\frac{1}{2},m}-T_{x,z}^{n+\frac{1}{2},m}\frac{\delta t\, T_{z,y}^{n+\frac{1}{2},m}}{\varepsilon_{zz}}\right]+\eta_{xz}T_{z,y}^{n+\frac{1}{2},m}\right)E_y^{n,m},$$

$$\gamma_y^{n+\frac{1}{2},m} = E_y^{n,m}+\frac{\delta t}{\mu_0}\left(\eta_{yy}\frac{B_x^{n+\frac{1}{2},m+\frac{1}{2}}-B_x^{n+\frac{1}{2},m-\frac{1}{2}}}{\delta z}\right)-\eta_{yy}\delta t\, T_y^{n+\frac{1}{2},m}+\delta t\left[\eta_{yy}\left(\frac{P_z^{n,m}}{\varepsilon_{zz}}-E_z^{n,m}\right)T_{y,z}^{n+\frac{1}{2},m}\right]$$
$$-\delta t\left(\eta_{yy}\left[T_{y,x}^{n+\frac{1}{2},m}-T_{y,z}^{n+\frac{1}{2},m}\frac{\delta t\, T_{z,x}^{n+\frac{1}{2},m}}{\varepsilon_{zz}}\right]\right)E_x^{n,m}+(\delta t)^2\frac{\eta_{yy}}{\varepsilon_{zz}}T_{y,z}^{n+\frac{1}{2},m}T_{z,y}^{n+\frac{1}{2},m}E_y^{n,m}+(\delta t)^2\frac{\eta_{yy}}{\varepsilon_{zz}}T_{y,z}^{n+\frac{1}{2},m}T_z^{n+\frac{1}{2},m}.$$

We write the linear system on $E_x^{n+1,m}$ and $E_y^{n+1,m}$

$$\left[1-\delta t\left(\eta_{xx}\frac{\delta t\, T_{z,x}^{n+\frac{1}{2},m}+\varepsilon_{zx}}{\varepsilon_{zz}}T_{x,z}^{n+\frac{1}{2},m}-\eta_{xz}T_{z,x}^{n+\frac{1}{2},m}\right)\right]E_x^{n+1,m}$$
$$+\delta t\left(\eta_{xx}\left[T_{x,y}^{n+\frac{1}{2},m}-T_{x,z}^{n+\frac{1}{2},m}\frac{\delta t\, T_{z,y}^{n+\frac{1}{2},m}}{\varepsilon_{zz}}\right]+\eta_{xz}T_{z,y}^{n+\frac{1}{2},m}\right)E_y^{n+1,m}=\gamma_x^{n,m}, \tag{3.6}$$
$$\delta t\eta_{yy}\left[T_{y,x}^{n+\frac{1}{2},m}-T_{y,z}^{n+\frac{1}{2},m}\frac{\delta t\, T_{z,x}^{n+\frac{1}{2},m}+\varepsilon_{zx}}{\varepsilon_{zz}}\right]E_x^{n+1,m}+\left[1-\delta t\left(\eta_{yy}T_{y,z}^{n+\frac{1}{2},m}\frac{\delta t\, T_{z,y}^{n+\frac{1}{2},m}}{\varepsilon_{zz}}\right)\right]E_y^{n+1,m}=\gamma_y^{n,m}.$$

This system has to be solved for each time-step. To simplify the previous expression, we rewrite the system as

$$\alpha_1^{n+\frac{1}{2},m}E_x^{n+1,m}+\delta t\alpha_2^{n+\frac{1}{2},m}E_y^{n+1,m}=\gamma_x^{n+\frac{1}{2},m},$$
$$\delta t\alpha_3^{n+\frac{1}{2},m}E_x^{n+1,m}+\alpha_4^{n+\frac{1}{2},m}E_y^{n+1,m}=\gamma_y^{n+\frac{1}{2},m},$$

the coefficients $\alpha_1^{n+\frac{1}{2},m}$, $\alpha_2^{n+\frac{1}{2},m}$, $\alpha_3^{n+\frac{1}{2},m}$ and $\alpha_4^{n+\frac{1}{2},m}$ depending only on variables computed before time $t^{n+\frac{1}{2}}$.

Remark 5. The density matrix ρ is bounded and so are the functions $T_{d_1,d_2}^{n+\frac{1}{2},m}$, for all directions d_1, d_2 and time n. Thus the determinant of system (3.6) goes to 1 as δt goes to 0. For reasonably small values of δt, system (3.6) is not singular.

At each step of the scheme derivation, we take care to make only approximations of at least order 2.

Proposition 6. *The following discretization scheme is of order two.*

$$\rho^{n+\frac{1}{2}} = S_{\mathscr{H}_0}^{\frac{1}{2}} S_{\mathscr{H}} S_{\mathscr{H}_0}^{\frac{1}{2}} \rho^{n-\frac{1}{2}},$$

$$\frac{B_x^{n+\frac{1}{2},m+\frac{1}{2}} - B_x^{n-\frac{1}{2},m+\frac{1}{2}}}{\delta t} = \frac{E_y^{n,m+1} - E_y^{n,m}}{\delta z},$$

$$\frac{B_y^{n+\frac{1}{2},m+\frac{1}{2}} - B_y^{n-\frac{1}{2},m+\frac{1}{2}}}{\delta t} = -\frac{E_x^{n,m+1} - E_x^{n,m}}{\delta z},$$

$$\begin{pmatrix} E_x^{n+1,m} \\ E_y^{n+1,m} \end{pmatrix} = \begin{pmatrix} \alpha_1^{n+\frac{1}{2},m} & \delta t \alpha_2^{n+\frac{1}{2},m} \\ \delta t \alpha_3^{n+\frac{1}{2}} & \alpha_4^{n+\frac{1}{2}} \end{pmatrix}^{-1} \begin{pmatrix} \gamma_x^{n+\frac{1}{2},m} \\ , \gamma_y^{n+\frac{1}{2},m} \end{pmatrix},$$

*where the operators $S_{\mathscr{H}_0}$ and $S_{\mathscr{H}}$ were defined during the derivation of the splitting of Bloch equation (*3.5*) in the previous section and the coefficients α_1, α_2, α_3, α_4, γ_x and γ_y in Eqs. (*3.6*).*

4. Boundary conditions

The equations describing the propagation of a laser pulse in our medium are then fully discretized. We now have to write the various boundary conditions before running some numerical experiences.We consider that before traveling through the medium, the wave-field propagates through a linear medium as shown in Fig. 1. This greatly simplifies the boundary conditions and the introduction of an incident wave.

4.1. Boundary conditions

To approach the physical conditions, in which the boundaries are transparent for the wave, we shall use the classical Silver–Müller condition. We use the discretization described in [11,23]. We denote by $\tilde{c}$ the speed of light in the linear medium.

At the domain entry, this is written as

$$\mathbf{E} - \mathbf{E}_\mathrm{i} - \tilde{c}(\mathbf{B} - \mathbf{B}_\mathrm{i}) \times \mathbf{n} = 0,$$

where $(\mathbf{E}_\mathrm{i}, \mathbf{B}_\mathrm{i})$ is the incident electromagnetic field, $\mathbf{n}$ is the outer normal vector to the domain.

The exit condition is written as

$$\mathbf{E} - \tilde{c}\mathbf{B} \times \mathbf{n} = 0.$$

By detailing for each coordinate, it gives

$$E_x - \tilde{c}B_y = 0,$$
$$E_y + \tilde{c}B_x = 0,$$

at the right boundary (exit) of the domain and

$$E_x - E_{i,x} + \tilde{c}(B_y - B_{i,y}) = 0,$$
$$E_y - E_{i,y} - \tilde{c}(B_x - B_{i,x}) = 0,$$

at the left boundary of the domain.

This raises a problem since the fields **E** and **B** are not discretized on the same points.

In a first step, let us study the case of the right boundary. As the magnetic field **B** is discretized on points interior to the domain, we need to discretize as **B** in space

$$E_x(t)^{M-\frac{1}{2}} - \tilde{c}B_y^{M-\frac{1}{2}} = 0,$$
$$E_y(t)^{M-\frac{1}{2}} + \tilde{c}B_x^{M-\frac{1}{2}} = 0,$$

which we approximate by

$$\frac{1}{2}(E_x(t)^{M-1} + E_x(t)^M) - \tilde{c}B_y^{M-\frac{1}{2}} = 0,$$
$$\frac{1}{2}(E_y(t)^{M-1} + E_y(t)^M) + \tilde{c}B_x^{M-\frac{1}{2}} = 0.$$

For the time variable, we discretize as the electric field **E**, i.e. for integer values of the time

$$\frac{1}{2}(E_x^{n+1,M-1} + E_x^{n+1,M}) - \frac{1}{2}\tilde{c}(B_y^{n+\frac{1}{2},M-\frac{1}{2}} + B_y^{n+\frac{3}{2},M-\frac{1}{2}}) = 0,$$
$$\frac{1}{2}(E_y^{n+1,M-1} + E_y^{n+1,M}) + \frac{1}{2}\tilde{c}(B_x^{n+\frac{1}{2},M-\frac{1}{2}} + B_x^{n+\frac{3}{2},M-\frac{1}{2}}) = 0.$$

At this stage, the values of the magnetic field **B** at time $n+\frac{3}{2}$ are not computed. Therefore, using the Faraday equations (2.8), we get

$$B_x^{n+\frac{3}{2},M-\frac{1}{2}} = B_x^{n+\frac{1}{2},M-\frac{1}{2}} + \frac{\delta t}{\delta z}(E_y^{n+1,M} - E_y^{n+1,M-1}),$$
$$B_y^{n+\frac{3}{2},M-\frac{1}{2}} = B_y^{n+\frac{1}{2},M-\frac{1}{2}} - \frac{\delta t}{\delta z}(E_x^{n+1,M} - E_x^{n+1,M-1}).$$

Finally, we obtain

$$E_x^{n+1,M} = \frac{1}{1+\frac{\tilde{c}\delta t}{\delta z}}\left(2\tilde{c}B_y^{n+\frac{1}{2},M-\frac{1}{2}} - \left(1 - \frac{\tilde{c}\delta t}{\delta z}\right)E_x^{n+1,M-1}\right),$$
$$E_y^{n+1,M} = \frac{1}{1+\frac{\tilde{c}\delta t}{\delta z}}\left(-2\tilde{c}B_x^{n+\frac{1}{2},M-\frac{1}{2}} + \left(-1 + \frac{\tilde{c}\delta t}{\delta z}\right)E_y^{n+1,M-1}\right).$$

Using the same method, we can express the condition at the left boundary

$$E_x^{n+1,1} = \frac{-1}{1+\tilde{c}\frac{\delta t}{\delta z}}\left(2\tilde{c}B_y^{n+\frac{1}{2},\frac{3}{2}} + \left(1 - \tilde{c}\frac{\delta t}{\delta z}\right)E_x^{n+1,2} - 2E_{i,x}^{n+1,1} - 2\tilde{c}B_{i,y}^{n+1,1}\right),$$
$$E_y^{n+1,1} = \frac{1}{1+\tilde{c}\frac{\delta t}{\delta z}}\left(2\tilde{c}B_x^{n+1,\frac{3}{2}} - \left(1 - \tilde{c}\frac{\delta t}{\delta z}\right)E_y^{n+1,2} + 2E_{i,y}^{n+1,1} - 2\tilde{c}B_{i,x}^{n+1,1}\right).$$

Remark 7. There is no need for additional relations to satisfy the conditions of continuity across the interface between the crystal and the linear medium (see Fig. 1).

5. Numerical experimentations

In order to validate the scheme and the corresponding code, let us proceed with several experimentations. In a first step, we restrict ourselves to the isotropic case and compare the code with results obtained in [5]. We then study some aspects of the anisotropy. Finally, we use the code in the specific case of a KDP crystal. More experimentations (such as self-induced transparency as in [24]) can be found in [20].

5.1. Isotropy and degeneracy

In this experiment, we consider a model with two distinct energy levels and four states. The lowest level is threefold degenerate. Each state of the lowest level is coupled with the second level in only one direction. The full description is given in Fig. 3. All other connections vanish.

Remark 8. Compared to the classical case of two level atoms with non-degenerate eigenvalues as in [27], this case really describes an isotropic medium. In [27] indeed, the direction corresponding to the unique non-vanishing vector of the dipolar moment matrix is predominant. One can overcome this difficulty by a posteriori choosing this direction parallel to the incoming electric field **E**. Thus for *this* polarization, the material acts as an isotropic medium. The model we present does not favor any direction of the polarization.

We take the following dipolar moment matrix $\boldsymbol{\mu}$ in (2.3)

$$\boldsymbol{\mu} : 10^{-29} \begin{pmatrix} 0 & 0 & 0 & \begin{pmatrix}1\\0\\0\end{pmatrix} \\ 0 & 0 & 0 & \begin{pmatrix}0\\1\\0\end{pmatrix} \\ 0 & 0 & 0 & \begin{pmatrix}0\\0\\1\end{pmatrix} \\ \begin{pmatrix}1\\0\\0\end{pmatrix} & \begin{pmatrix}0\\1\\0\end{pmatrix} & \begin{pmatrix}0\\0\\1\end{pmatrix} & 0 \end{pmatrix} \text{C.m.}$$

Hence the medium should act as an isotropic crystal. Let us try several angles for the incoming wave to prove this fact. We take a powerful (10^8 V/m) and short (1 fs) Gaussian laser pulse propagating through 25 μm of the medium.

When only changing the two angles θ and ϕ, the result remains exactly the same. For instance, let us take zero for θ and ϕ.

The results are similar for any angle θ or ϕ and for the other physical values considered (such as the density matrix). Numerically, the medium acts effectively as an isotropic medium (see Figs. 4 and 5).

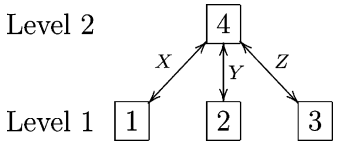

Fig. 3. Connections between atomic levels.

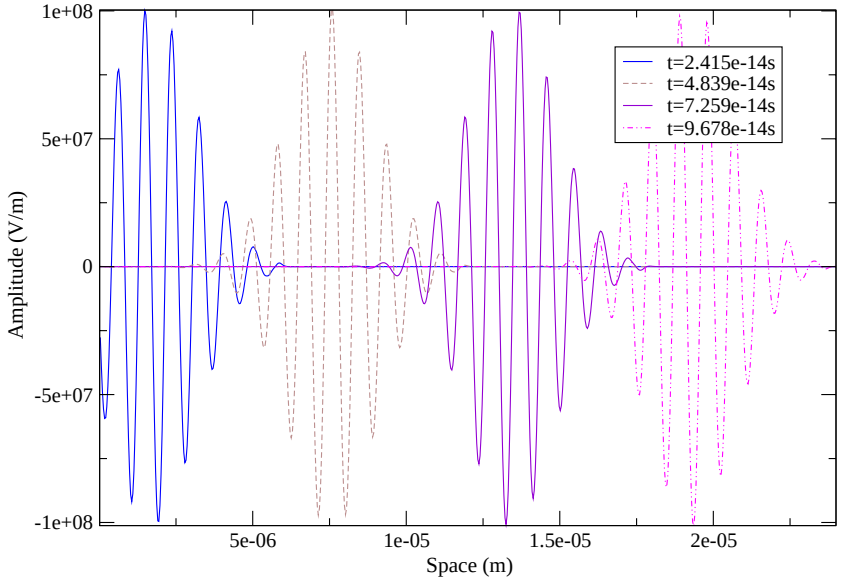

Fig. 4. Evolution of the electric field for $\theta = 0.7173303$ and $\phi = 0.78$ in an isotropic medium.

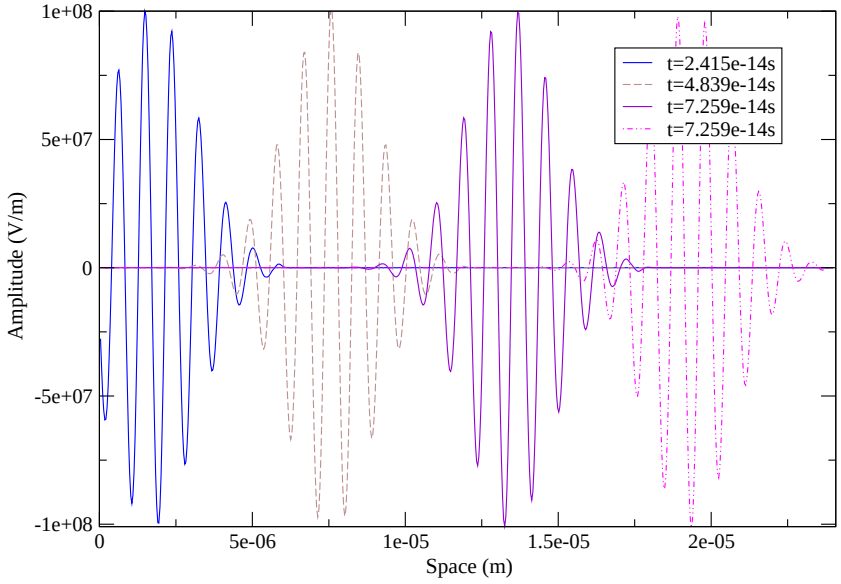

Fig. 5. Evolution of the electric field for $\theta = 0$ and $\phi = 0$ in an isotropic medium.

5.2. Propagation in a KDP crystal

In [4], we described a Maxwell–Bloch model for wave-propagation in nonlinear crystals applied to the KDP crystal. Compared to macroscopic models like [7], this microscopic model accounts for microscopic physics in a fairly accurate way. A true difficulty in this microscopic approach was to obtain all the

microscopic information on the quantum structure of the crystal. Indeed, the only available data on the crystal are linear and quadratic susceptibilities from [10,13–16,18,22,26] for instance, and its group of symmetry [1]. In [4], we had to recover microscopic information such as the dipolar moment matrix $\boldsymbol{\mu}$ from the dispersion properties of the material. We first related the first and second order susceptibilities to the dipolar moment matrix as in [8]. We then postulated the most simple quantum-state structure able to reproduce the symmetry and anisotropy properties of the KDP. In the model described [4], the nonlinear effects are not restricted to linear and quadratic ones as in the case of many models based on optical susceptibilities. However, microscopic model simulations are much more computationally expensive.

Since the writing of [4], we have found that the model is quite sensible to the parameters. Indeed for small densities $\mathscr{N}$, we have to take a rather fine mesh to obtain satisfying results. The dipolar matrix $\boldsymbol{\mu}$ is computed from the density $\mathscr{N}$ and the linear and quadratic susceptibilities of the crystal [4]. The origin of this problem is difficult to find as there are many phenomena involved (numerical dispersion disturbing the phase matching, the effects of optical rectification exciting lower frequencies, the simplicity of our model which leads to large elements in the dipolar moment matrix $\boldsymbol{\mu}\ldots$).

For the following runs, we have taken $\mathscr{N} = 1.103272714 \times 10^{30}$, $\omega_{21} = 4.712388980 \times 10^{13}$ Hz, $\omega_{31} = 1.674041079 \times 10^{16}$ Hz, $\mu^1_{(1,2)} = -0.153314735 \times 10^{-28}$ m and $\mu^3_{(3,2)} = -0.756543053 \times 10^{-29}$ m. The remaining elements of the dipolar matrix $\boldsymbol{\mu}$ are computed by the relations written in [4]. We take 100 points per wavelength (and thus 50 in the second harmonic). For these parameters, the results do not change with finer meshes or smaller time steps.

The crystal is surrounded with a linear material. In practice, the medium parameters are chosen so as to minimize the reflexion of the wave at the interfaces with the KDP. In the following figures, the wave is only plotted inside the crystal.

5.2.1. A Pockels cell

In this experiment, a static electric field is applied in the crystal. We show an effect of the quadratic susceptibility of the crystal known as the Pockels effect. This static field is parallel to the direction of propagation z, which is also the direction of the optical axis of the crystal. We take a field of 10^9 V/m. The incoming wave is a short (20 fs) Gaussian pulse, whose max value is 10^3 V/m. The angle of incidence is zero.

Because of the static field, the polarization of the incoming wave will rotate as it propagates through the crystal. We obtain a Pockels cell [9]. The incoming wave is polarized along the direction **y**. As the wave propagates, the polarization rotates as shown in Fig. 6. After 23 μm, the wave is almost entirely polarized along the **x** direction.

As expected, we observe a rotation of the polarization in Fig. 6.

5.2.2. Second harmonic generation

To further check the capabilities of our numerical method, let us study the second harmonic generation of an ultrashort Gaussian pulse in a KDP crystal.

In [7], a similar experience is performed using a model based on nonlinear Maxwell equations. In this run, the electric field **E** is a Gaussian pulse of amplitude 10^{10} V/m lasting 20 fs. We use the model described in [4], which gives a dipolar matrix $\boldsymbol{\mu}$ for a KDP crystal from the macroscopic susceptibilities of the crystal obtained from [26].

Since we want to observe second harmonic generation, the phase matching condition has to be satisfied. For the second harmonic, in the KDP, the values of angles between the direction of propagation of the wave and the optical axes of the crystal are, for a phase match of type I [7], $\theta = 41°$, $\phi = 45°$. The crystal is rotated to ensure the phase match. Finally, in order to keep a normal incidence for the wave, the crystal is cut perpendicularly to the direction of propagation.

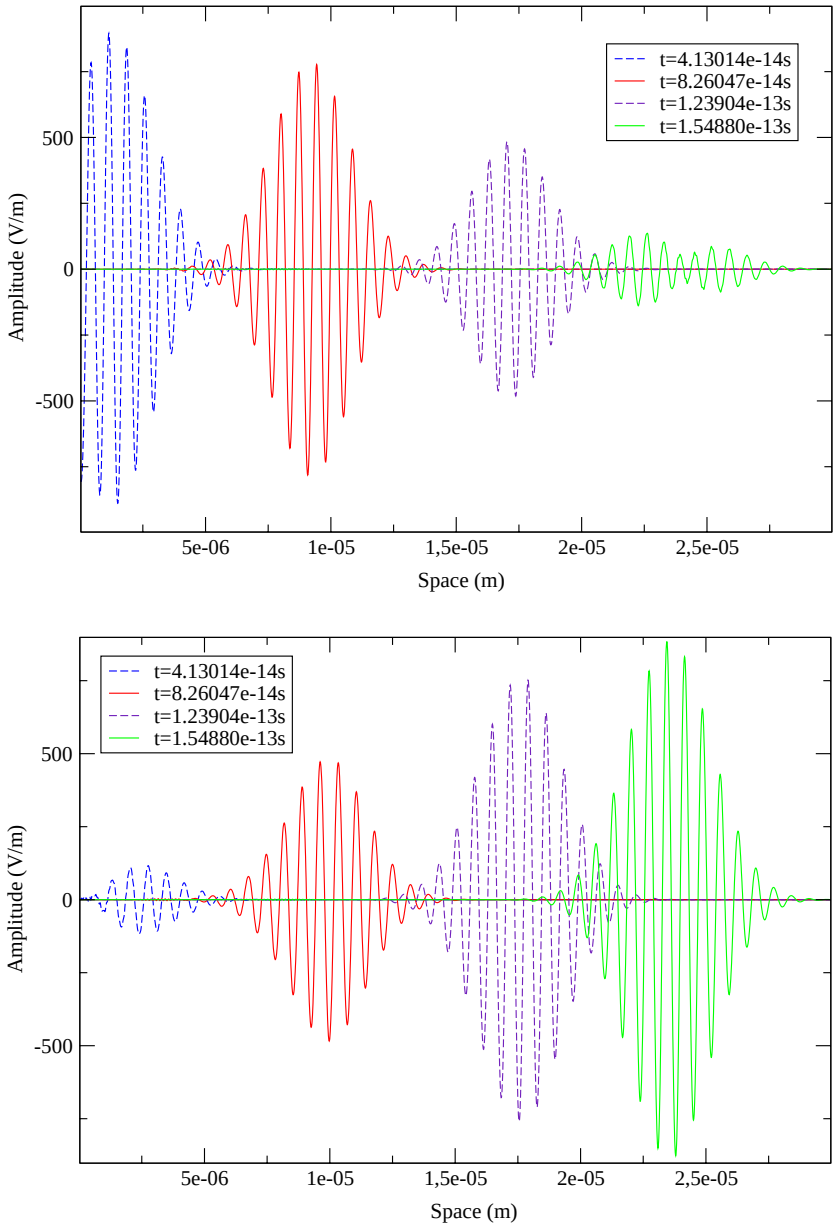

Fig. 6. Evolution of the electric field (E_y and E_x) in a Pockels cell.

The electric field **E** is polarized along the y-axis. The second harmonic wave and all harmonics of even order should appear in the x-axis. Cubic harmonic and greater odd harmonics should also be observed along the y axis.

First, as shown in Fig. 7, the evolution of the second coordinate of the electric field is plotted for different times. The intensity of the field decreases as the light travels the crystal (as the length of propagation is short, this effect is rather difficult to observe).

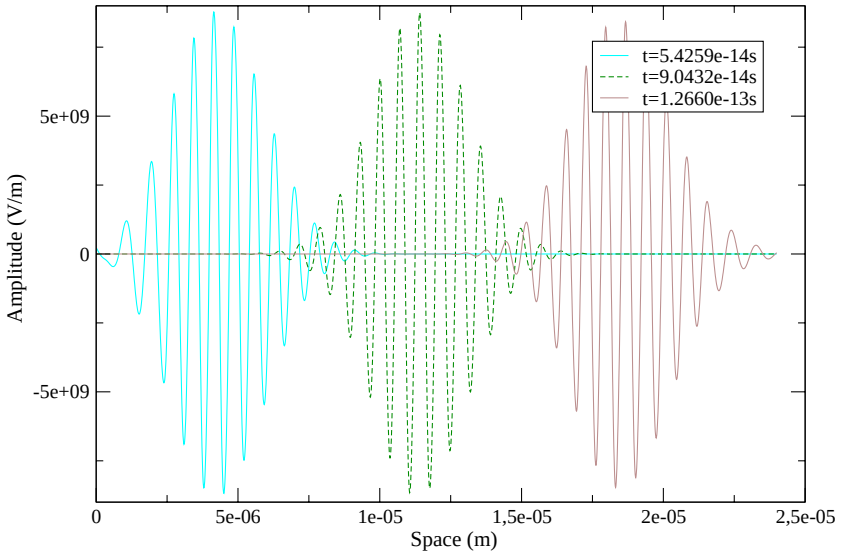

Fig. 7. Evolution of the component E_y of the electric field **E** in an experiment of second harmonic generation at the phase matching angle.

We now consider the Fourier transform of the wave field. The unit of frequency corresponds to the frequency of the incoming wave. In the y-coordinate (as shown in Fig. 8), the amplitude of the Fourier transform corresponding to the frequency of the incoming wave decreases as the wave travels through the crystal. Moreover, third harmonic generation is observed.

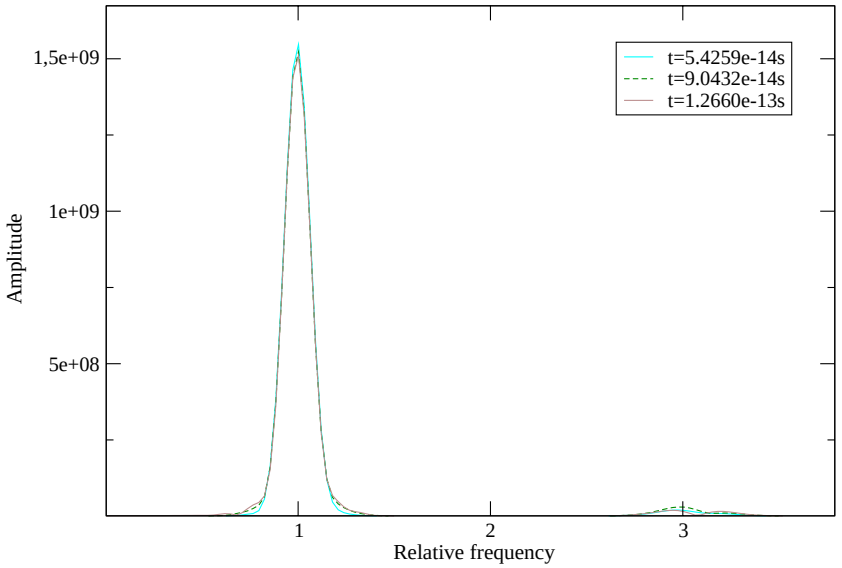

Fig. 8. Evolution of the Fourier transform of the component E_y of the electric field **E** (which should contain odd harmonics) in an experiment of second harmonic generation at the phase matching angle.

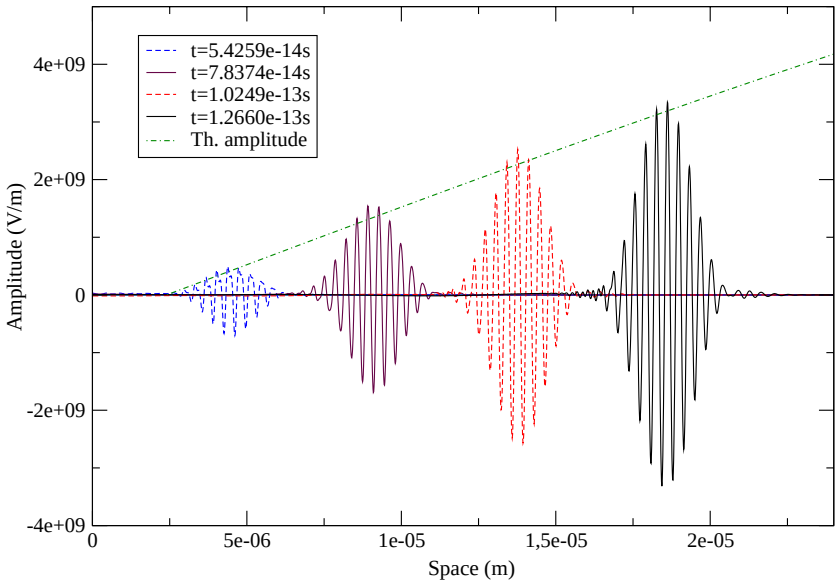

Fig. 9. Evolution of the component E_x of the electric field **E** in an experiment of second harmonic generation at the phase matching angle.

We then show the evolution of E_x. At the initial time, there is no field along this coordinate as the wave is initially polarized along the y direction. But as the wave goes through the crystal, the amplitude of this component increases, as shown in Fig. 9, where the electric field E_x is drawn at various times. At the phase matching angle, the intensity of the second harmonic increases with z. We have also plotted the theoretical amplitude (see Chapter 2 of [8] for detail) of the second harmonic, thus we can visualize the accuracy of our model.

In Fig. 10, we have plotted the Fourier transform of E_x at different times. The frequency plotted is relative to the frequency of the incoming wave. Over time, the intensity of the second harmonic increases. We can also observe the appearance of a weak fourth harmonic and the effect of optical rectification in the lower frequencies of the spectrum.

So far, the numerical results are those expected and are similar to the results obtained by macroscopic models such as in [7] for the first two nonlinear effects. In this experience, we have observed higher nonlinearities than the linear and quadratic ones, which are the only ones observable by classical nonlinear Maxwell model such as in [7].

To push the test a little further, we change the angle of the wave and carry out the same experiment. The phase matching condition is no longer satisfied, we take $\theta = 29.64°$, $\phi = 33.54°$. In Fig. 11, we plotted the electric field for ten different times. As there is no phase matching any longer, the second harmonic is destroyed before the wave leaves the crystal.

At the beginning of the experiment, the intensity of the field E_y decreases as in Fig. 7. But as time goes on, the effects of the phase mismatch start to affect the wave and the second harmonic is turned back into the fundamental harmonic.

As we could have expected, in Fig. 11, the intensity of the field starts by increasing but after a certain time, it goes to zero.

To compute the coherency length, we inject a sinusoidal wave in the crystal in order to have a monochromatic wave. To reduce the effects of higher nonlinearities, we take a field **E** of 10^5 V/m. The coherency

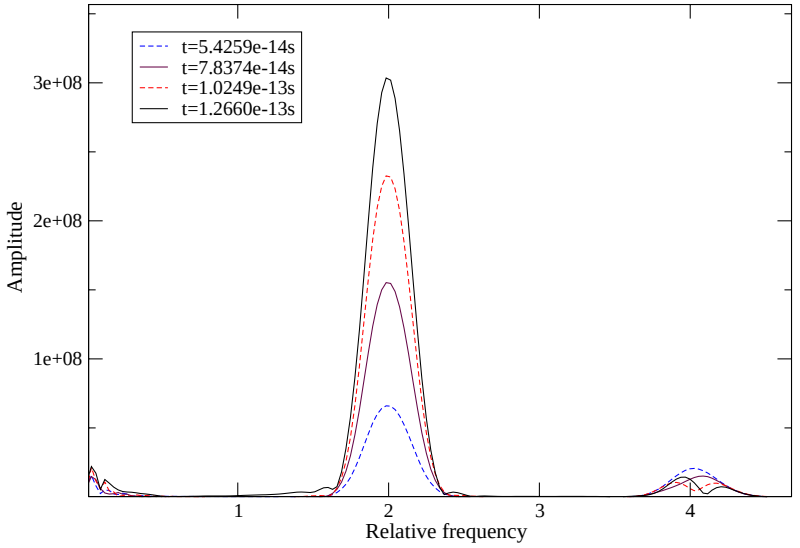

Fig. 10. Evolution of the Fourier transform of the component E_x of the electric field **E** (which should contain even harmonics) in an experiment of second harmonic generation at the phase matching angle.

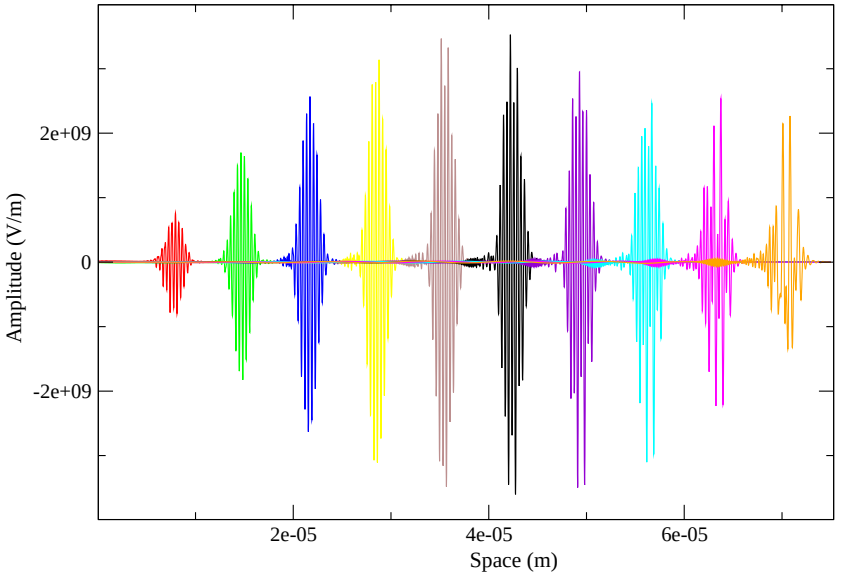

Fig. 11. Evolution of the component E_x of the electric field **E** when the phase matching condition is no longer satisfied. The electric field is plotted every 3.42058×10^{-17} s.

length is equal to half the distance between knots of E_x. For this experiment, we computed a coherency length of 33.8 μm. In Fig. 12, we have plotted the first component of the electric field containing the second harmonic after 4.195×10^{-13} s.

Finally, we have obtained the results expected.

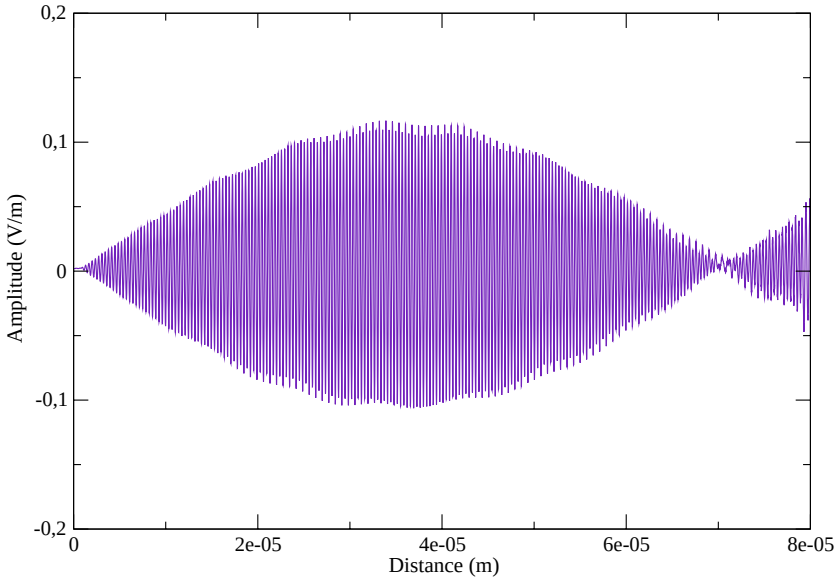

Fig. 12. Evolution of the component E_x of the electric field **E** when the phase matching condition is not satisfied. The incoming wave is sinusoidal.

6. Conclusion

In this paper, we derived a scheme for the Bloch model in the case of anisotropic media. We had to extend the existing scheme [5,27] used for isotropic media. Another problem was to examine the angle between the direction of the wave propagation and the optical axis of the crystal, in order to study the phase mismatch effects on the wave.

Besides, we attempted to keep a reasonably accurate scheme, by describing the steps needed to ensure a second order scheme. We also wrote the boundary and interface relations for our model. Once the scheme written, we proceeded with numerical experiments ranging from the case of an isotropic medium to a complete simulation of the propagation of a laser pulse through a crystal of KDP. As the model offered in [4] can be usually extended to a large class of materials, the scheme described in this paper could also be applied to various anisotropic media.

However, this model involves heavy numerical computations, especially in the solving of Ampère (2.6) and Bloch (2.5) equations. It shall thus be used either for short propagation distance or as a validation tool for simpler macroscopic models. For instance, it could be useful in finding dispersion relations for non-linear Maxwell models as in [7]. However, the computation times shall be significantly reduced. Indeed, the Bloch equation (2.5) can easily be parallelized: the space variable acts as a parameter, the computations for each space-step could be performed at the same time. The second bottleneck in term of performance is the resolution of the Ampère system of Eqs. (2.6). Even if some simple improvements can clearly be obtained through parallelism, this parallelization is beyond the scope of this article.

Acknowledgements

The author thanks Christophe Besse, Antoine Bourgeade and Pierre Degond for their invaluable help during this work.

References

[1] P.W. Atkins, R.S. Friedman, Molecular Quantum Mechanics, Oxford University Press, Oxford, 1996.
[2] H.J. Bakker, P.C.M. Planken, L. Kuipers, A. Lagendijk, Phase modulation in second-order nonlinear-optical processes, Phys. Rev. A 42 (7) (1990) 4085–4101.
[3] H.J. Bakker, P.C.M. Planken, H.G. Muller, Numerical calculation of optical frequency-conversion processes: a new approach, J. Opt. Soc. Am. B 6 (9) (1989) 1665–1672.
[4] C. Besse, B. Bidégaray, A. Bourgeade, P. Degond, O. Saut, A Maxwell–Bloch model with discrete symmetries for wave propagation in nonlinear crystals: an application to KDP (submitted).
[5] B. Bidégaray, Time discretizations for Maxwell–Bloch equations, Numer. Meth. Partial Differential Equations 19 (2003) 284–300.
[6] B. Bidégaray, A. Bourgeade, D. Reignier, Introducing physical relaxation terms in Bloch equations, J. Comput. Phys. 170 (2) (2001) 603–613.
[7] A. Bourgeade, E. Freysz, Computational modeling of second-harmonic generation by solution of full-wave vector Maxwell equations, J. Opt. Soc. Am. B 17 (2) (2000) 226–234.
[8] R.W. Boyd, Nonlinear Optics, Academic Press, New York, 1992.
[9] B. Cagnac, J.P. Faroux, Lasers, Interactions lumière-atomes, EDP Sciences, 2002.
[10] M.M. Choy, R.L. Byer, Accurate second-order susceptibility measurements of visible and infrared nonlinear crystals, Phys. Rev. B 14 (4) (1976) 1693–1706.
[11] F. Deluzet, Modélisation mathématique et simulation numérique de commutateurs d'ouverture à plasma, Ph.D. Thesis, 2002.
[12] T. Ditmire, A.M. Rubenchik, D. Eimerl, M.D. Perry, Effects of cubic nonlinearity on frequency doubling of high-power laser pulses, J. Opt. Soc. Am. B 13 (4) (1996) 649–655.
[13] R. Eckardt, H. Masuda, Y.X. Fan, R.L. Byer, Absolute and relative nonlinear optical coefficients of KDP, KDP*, BaB_2O_4, $LiIO_3$, MgO: $LiNbO_3$ and KTP measured by phase-matched second-harmonic generation, IEEE J. Quantum Electron. 26 (5) (1990) 922–933.
[14] D. Eimerl, Electro-optic, linear and nonlinear optical properties of KDP and its isomorphs, Ferroelectrics 72 (1987) 95–139.
[15] J. Jerphagnon, S.K. Kurtz, Optical nonlinear susceptibilities: accurate relative values for quartz, ammonium dihydrogen phosphate, potassium dihydrogen phosphate, Phys. Rev. B 1 (4) (1970) 1739–1744.
[16] K.W. Kirby, C.S. Hoeffer, L.G. Deshazer, Refractive indices and thermo-optic coefficients on nonlinear crystals isomorphic to KDP, Final Report, Lawrence Livermore National Laboratory, 1985.
[17] N.C. Kothari, X. Carlotti, Transient second-harmonic generation: influence of effective group-velocity dispersion, J. Opt. Soc. Am. B 5 (4) (1988) 756–764.
[18] S.K. Kurtz, J. Jerphagnon, M.M. Choy, Nonlinear dielectric susceptibilities, Landolt–Boernstein New Series 3 (11) (1979) 671–743.
[19] R. Maleck Rassoul, A. Ivanov, E. Freysz, A. Ducasse, F. Hache, Second-harmonic generation under phase-velocity and group-velocity mismatch: influence of cascading self-phase and cross-phase modulation, Opt. Lett. 22 (5) (1997) 268–270.
[20] O. Saut, Etude numérique des nonlinéarités d'un cristal par résolution des équations de Maxwell–Bloch, Ph.D. Thesis, INSA Toulouse, 2003.
[21] L.I. Schiff, Quantum Mechanics, McGraw-Hill International Editions, 1995.
[22] I. Shoji, T. Kondo, A. Kitamoto, M. Shirane, R. Ito, Absolute scale of second-order nonlinear-optical coefficients, J. Opt. Soc. Am. B 14 (9) (1997) 2268–2294.
[23] A. Taflove, S.C. Hagness, Computational Electrodynamics: The Finite-difference Time-domain Method, second ed., Artech House, Boston, MA, 2000.
[24] A. Yariv, Quantum Electronics, Wiley, New York, 1989.
[25] K.S. Yee, Numerical solution of initial boundary value problems involving Maxwell's equations in isotropic media, IEEE Trans. Antennas Propag. AP-14 (1966) 302–307.
[26] F. Zernicke, Refractive indices of ADP and KDP between 2000 Å and 1.5 μm, J. Opt. Soc. Am. 54 (10) (1964) 1215–1220.
[27] R.W. Ziolkowski, J.M. Arnold, D.M. Gogny, Ultrafast pulse interactions with two-level atoms, Phys. Rev. A 52 (4) (1995) 3082–3094.